Application and Optimization of Passive Wireless Temperature Measurement Technology in Rotor Monitoring of Generator-Motor

Bi Yang¹#Zhifu Xiong¹ Hongyu Sun¹ Jiawen Li¹ Shuang Peng¹ Dong Zhang²*

- 1. Chongqing Panlong Pumped Storage Power Station Co., Ltd
 - 2. Dongfang Electric Group Dongfang Electric Co., Ltd First Author#:Bi Yang

Contact*:Dong Zhang yeyu757463274@163.com。Password: Zd181977.

Bi Yang: 4316101@qq.com

Zhifu Xiong: 873468227@qq.com

Hongyu Sun: <u>2775352144@qq.com</u>

Jiawen Li: 896340171@qq.com

Shuang Peng: 493871559@qq.com

Dong Zhang: yeyu757463274@163.com

Fund: State Grid Xinyuan Group Co., Ltd. Science and Technology Project Funding, Project No. SGXYKJ-2022-078

Abstract: Temperature monitoring of generator-motor rotor is extremely challenging under conditions of high temperature, high-speed rotation, and strong electromagnetic interference. In response to this requirement, a passive wireless temperature measurement system based on Ultra-High Frequency (UHF) RFID is developed. This system realizes passive transmission of temperature data through electromagnetic coupling of RFID technology. Structurally, it adopts a multi-antenna layout and dynamic threshold adjustment to enhance the system's anti-interference capability and monitoring stability. Experimental results indicate that within a threshold range of 0.4 to 0.6, the system's sensitivity reaches 91.07%-94.44%, with specificity exceeding 91.84%. The relative error of the Long Short-Term Memory (LSTM) prediction model is below 1.5%, significantly improving the accuracy of temperature anomaly detection. In summary, this technical solution is suitable for real-time rotor temperature monitoring and fault early warning in complex environments.

Keywords: Generator-motor rotor; Passive wireless temperature measurement;

Temperature sensor; Time series prediction; Pumped storage power station

During the operation of generator-motor, the rotor operates in a high-speed rotation and high-temperature environment, accompanied by intense electromagnetic interference. This poses significant challenges to traditional wired temperature measurement methods. Traditional wired temperature monitoring systems suffer from complex wiring, susceptibility to interference, and difficulties in maintenance, making it difficult to meet the real-time monitoring requirements in complex environments [1]. Therefore, passive wireless temperature measurement technology, which is highly stable, highly resistant to interference, and does not require external power support, has gradually gained attention [2].

In recent years, passive wireless temperature measurement systems based on RFID (Radio Frequency Identification) technology have been gradually applied in special scenarios such as high temperature and high-speed rotation. These systems achieve energy transmission and data acquisition through electromagnetic coupling, effectively enhancing monitoring stability and reliability while reducing equipment maintenance difficulty [3]. However, traditional RFID systems are prone to data loss or unstable transmission under high-speed rotation conditions, and lack intelligent early warning capabilities for temperature anomalies, unable to meet the real-time and precise monitoring requirements of rotor [4].

Current research mostly focuses on improving RFID reading distance and anti-interference capabilities, without optimization for the specific needs of high-speed rotating rotor environments, especially lacking effective methods for dynamic temperature change prediction and anomaly detection [5]. Therefore, it is necessary to design a stable, reliable, and real-time passive wireless temperature measurement system tailored to the actual requirements of generator-motor rotor temperature monitoring, and explore temperature prediction and early warning algorithms suitable for complex operating conditions, in order to achieve precise monitoring of rotor temperature and early fault warning.

1.Design of Application Scheme for Passive Wireless Temperature Measurement Technology in Generator-Motor Rotor

1.1 Technology Selection and System Composition

The application of passive wireless temperature measurement technology in generator-motor rotor necessitates overcoming challenges such as high-speed rotation, intense electromagnetic interference, and high-temperature environments. In terms of technology selection, the adoption of RFID passive wireless temperature measurement systems suitable for high-speed rotating structures is crucial. RFID technology does not require external power supply and relies on electromagnetic field coupling for energy transmission and data communication, boasting high stability and reliability [6]. By comparing several common passive wireless temperature measurement technologies, a solution based on Ultra-High Frequency (UHF) RFID was selected due to its excellent anti-interference capabilities and long reading distance, making it suitable for online temperature monitoring of rotor poles.

The main components of the system include temperature sensors, RFID reader/writer, antennas, and controllers. The temperature sensors are responsible for monitoring temperature changes in the rotor poles and transmitting temperature data to the readers/writers via antennas. The reader/writer antennas are installed on stationary components and communicate with the RFID tags on the rotor through electromagnetic coupling to complete data acquisition. The controller is responsible for data processing and communication with the host computer to achieve real-time monitoring and early warning of temperature data.

1.2 System Structure and Hardware Layout

In the system structure design, the preliminary layout scheme diagram for the real-time rotor pole temperature monitoring system is shown in Figure 1.

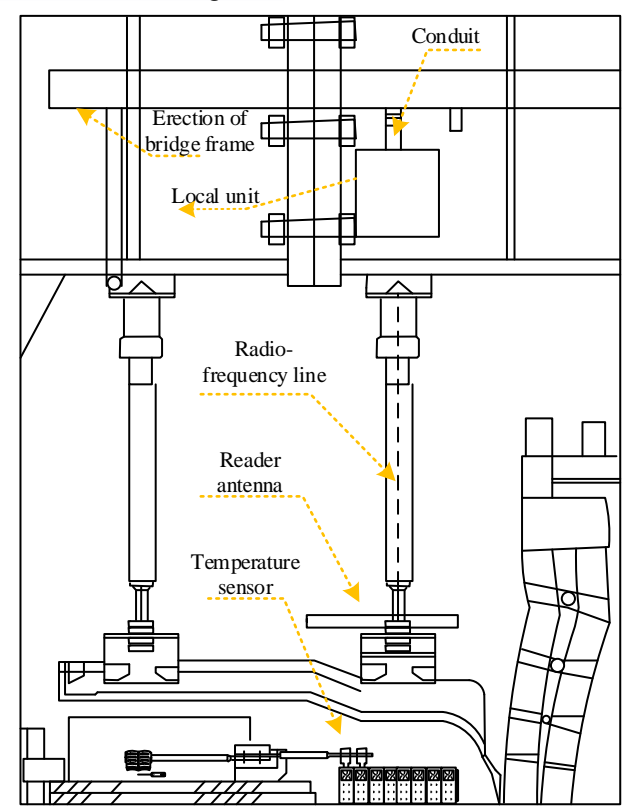


Fig. 1 Preliminary Layout Scheme for Real-Time Monitoring System of Rotor Pole Temperature

Temperature sensors are installed at the lead-out wires of the rotor poles through special fixing structures to ensure measurement accuracy and reliability. During sensor installation, mechanical strength and operational safety must be considered, utilizing high-strength, lightweight PCB thin board encapsulation to minimize the impact on the rotor structure.

The reader/writer antennas are arranged at suitable positions inside the stator, with consideration given to the optimization design of antenna gain and reading distance. To ensure data transmission stability under high-speed rotor rotation conditions, the system adopts a multi-antenna design to cover different angles of the rotor poles, reducing communication blind spots caused by changes in rotor position. Additionally, the reader are installed away from areas with strong electromagnetic interference to reduce noise interference during system operation.

The design principles for the layout of sensors and antennas include ensuring the accuracy of temperature data, maintaining the mechanical safety of the system, and avoiding the introduction of new risks due to installation. Therefore, the system network diagram is shown in Figure 2.

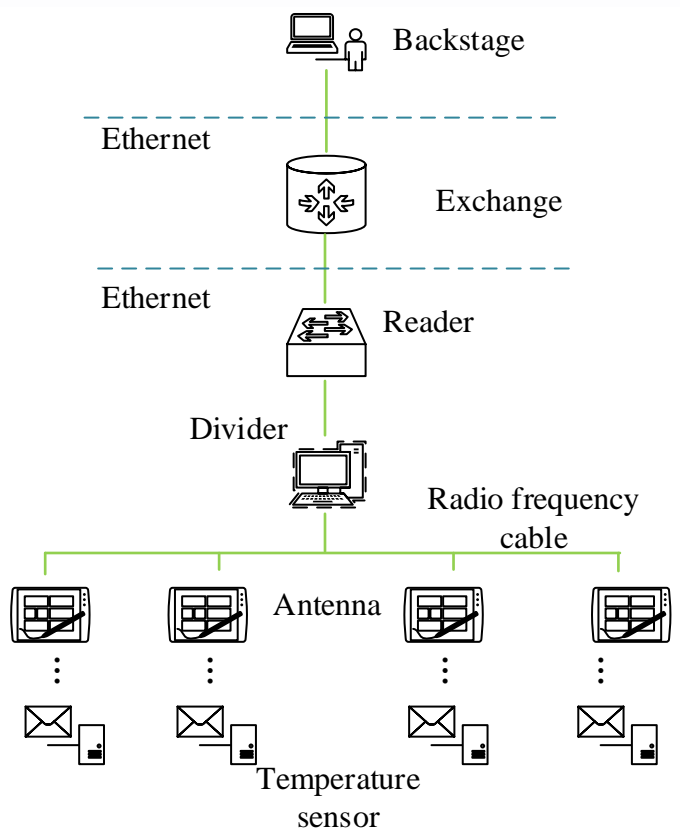


Fig. 2 System Network Diagram

1.3 Network Transmission and Data Processing

In the design of network transmission, the wireless temperature measurement system reads temperature data via temperature sensors and transmits it to the control center. Industrial-grade wireless network protocols are employed to ensure data reliability and real-time performance. During data acquisition, the RFID reader communicates with the temperature sensors at a set sampling frequency, and the read temperature data undergoes initial processing through an edge computing module, including data validation and filtering, to ensure data validity.

The real-time temperature data is transmitted to the host computer system via industrial Ethernet, supporting real-time display of temperatures and storage and querying of historical data. To further enhance the system's response speed, an event-triggered data acquisition mode is designed. When the temperature exceeds a set threshold, the system immediately transmits an early warning signal to notify operations and maintenance personnel for timely handling. This mode significantly reduces data redundancy, improves transmission efficiency, and enhances the system's real-time warning capabilities.

2. Algorithm Development

2.1Temperature Prediction Algorithm Based on Time Series

In this research, a Long Short-Term Memory (LSTM) neural network based on time series is employed to predict the rotor pole temperature of pumped storage units, aiming to achieve early fault warning. The LSTM model is capable of capturing the nonlinear dynamic characteristics in temperature variations. Its structure comprises forget gates, input gates, candidate memory, and output gates, which can retain critical information in long sequences, thereby enabling high-precision temperature prediction.

In LSTM, the input vector x_t at each time step interacts with the hidden state h_{t-1} from the previous time step to update the cell state t. The formula for updating the cell state is as shown in Equation (1).

$$c_t = f_t \cdot c_{t-1} + i_t \cdot \varsigma_t(1)$$

In this context, f_t and i_t represent the outputs of the forget gate and the input gate, respectively. f_t controls the degree of retention of the previous state c_{t-1} , while i_t controls the influence of the new input x_t on the current state c_t . ζ_t serves as the candidate memory cell, which applies a nonlinear transformation to the input information through the Tanh activation function, resulting in values within the range of -1 to 1. During the construction of the temperature prediction model, key parameters such as the number of layers and the number of hidden units have significant impacts on the prediction performance. Therefore, to optimize the model structure, this project introduces the Ant Colony Optimization (ACO) algorithm for parameter tuning. By simulating the behavior of ants searching for the optimal path in nature, ACO can effectively search for the optimal solution through iterations. ACO transforms the parameter selection problem of the temperature prediction model into a path optimization problem, enabling the model to automatically adjust to the best configuration during the parameter tuning phase.

In the ACO algorithm, each ant searches for a path in the parameter space, with the selection probability based on the heuristic information of the path and the distribution of pheromones already present on the path. In the path selection probability, the probability p_i^k of ant k choosing path i is influenced by the heuristic factor η_i and the pheromone concentration τ_i . The definitions are as follows:

$$p_i^k = \frac{(\tau_i)^{\alpha} (\eta_i)^{\beta}}{\sum_{j \in Allowed} (\tau_j)^{\alpha} (\eta_j)^{\beta}} (2)$$

In this context, α and β are weight parameters that regulate the pheromone and heuristic factors, respectively. η_i represents the heuristic information on path i (i.e., the expected benefit), which is directly proportional to the prediction accuracy of the model. After each iteration, the pheromone concentration on the

path is updated. Assuming that the pheromone concentration on path i is τ_i , the update formula is as follows.

$$\tau_i \leftarrow (1 - \rho)\tau_i + \Delta \tau_i(3)$$

In this context, ρ denotes the pheromone evaporation coefficient, which indicates the decay rate of pheromones. $\Delta \tau_i$ represents the amount of pheromone newly added to path i in the current search iteration.

The increment in pheromone, $\Delta \tau_i$, is typically proportional to the quality of path i, serving as a reward for the more optimal paths. The definitions are as follows.

$$\Delta \tau_i = Q / Cost_i(4)$$

In this context, Q is a constant, and $Cost_i$ denotes the "cost" of path i, which is typically the prediction error of the model under the path's parameters. During the parameter optimization process, the Mean Squared Error (MSE) is calculated as the evaluation criterion to measure the prediction performance of the LSTM model under the current parameter configuration. The definitions are as follows.

$$MSE = \frac{1}{n} \sum_{t=1}^{n} (y_t - \hat{y}_t)^2$$
 (5)

In this context, y_t represents the actual temperature, \hat{y}_t denotes the predicted temperature, and n is the number of samples. By minimizing the MSE value, the model gradually adjusts to the optimal parameter configuration. Ants progressively adjust their path selection based on the pheromone distribution and prediction errors. After multiple iterations, they ultimately converge to the optimal solution. The optimization objective is defined as follows.

$$\min MSE_{total} = \sum_{i=1}^{k} MSE(i) (6)$$

This objective accumulates the errors from multiple paths explored by the ants to find the optimal parameter combination that minimizes the mean squared error of temperature predictions. Therefore, guided by the ant colony algorithm, the model gradually converges to the optimal parameter settings during iterations, enabling the LSTM model to maintain high-precision temperature prediction outputs under varying environmental conditions, making it suitable for complex and dynamic temperature monitoring scenarios.

2.2 Anomaly Detection and Early Warning Algorithm

In the online monitoring of magnetic pole temperatures in pumped storage units, to promptly identify abnormal temperature rises and achieve intelligent early warning, an anomaly detection algorithm based on dynamic threshold adjustment is designed. This algorithm not only relies on the statistical characteristics of historical data but also utilizes the sliding window method and an anomaly identification mechanism based on the Z-Score to cope with the dynamic changes in temperature fluctuations.

In dynamic threshold and sliding window anomaly detection, the difference between normal and abnormal states of temperature changes is often manifested as abrupt changes in the temperature curve. Consequently, the anomaly detection algorithm employs the sliding window method to calculate the short-term mean μ_t and standard deviation σ_t of the temperature, dynamically reflecting the trend of temperature changes through rolling calculations. The mean and standard deviation of the temperature values within the sliding window are defined as follows.

$$\mu_{t} = \frac{1}{W} \sum_{i=t-W+1}^{t} T_{i}, \ \sigma_{t} = \sqrt{\frac{1}{W} \sum_{i=t-W+1}^{t} (T_{i} - \mu_{t})^{2}}$$
 (7)

In this context, W represents the window length, and T_i denotes the temperature value at time step i. μ_t and σ_t within the sliding window characterize the short-term fluctuations in temperature, aiding in real-time monitoring of temperature changes. At each time step, the current temperature T_t is compared with a dynamic threshold formed by the combination of μ_t and σ_t , and the degree of temperature anomaly is defined using the Z-Score.

$$Z_{t} = \frac{T_{t} - \mu_{t}}{\sigma_{t}} (8)$$

When $|Z_t| > \delta$, the temperature is deemed abnormal, where δ is a preset threshold typically ranging between 2 and 3. The calculation of the Z-Score dynamically reflects the degree of deviation of the temperature from its mean. The chosen δ value should take into account the noise in the temperature data to balance the false alarm rate and the missed detection rate. To accommodate long-term temperature trends while mitigating the impact of occasional fluctuations, the early warning model employs a two-tier detection structure. It leverages dynamic thresholds based on the sliding window for real-time monitoring and adjusts the δ value using the Exponential Weighted Moving Average (EWMA) in conjunction with historical temperature data trends. The given EWMA formula is as follows.

$$\delta_t = \alpha \cdot Z_{t-1} + (1 - \alpha) \cdot \delta_{t-1}(9)$$

Where α is the smoothing coefficient, typically ranging between 0.1 and 0.3. This method applies weighted processing to historical Z-Scores to adjust δ in real-time, enhancing the adaptability of the detection.

3. Experimental Analysis and Performance Validation

3.1 Experimental Platform and Testing Environment

To verify the practical monitoring performance of passive wireless temperature measurement technology

on generator-motor rotors, this experiment deployed a temperature sensor system within the rotor environment of a generator-motor at a pumped storage power station. The power station has an installed capacity of 1200MW (4×300MW), equipped with four single-stage vertical-shaft single-speed mixed-flow reversible pump-turbine electro-generator units, each with a unit capacity of 300MW. The rated speed is 428.6rpm, and the rated head under turbine conditions is 428m. The power station is connected to the Longsheng substation of Chongqing Power Grid via a single 500kV line with primary voltage. The experimental platform comprises RFID temperature sensors, RFID readers/writers, data acquisition equipment, and a control system. The testing environment is located in the high-speed rotating area of the rotor, where the ambient temperature fluctuates significantly, allowing for the assessment of the system's stability and reliability under high temperatures and strong electromagnetic interference. Experimental data is transmitted to the host computer via industrial Ethernet for real-time monitoring, storage, and analysis. The experimental equipment is listed in Table 1.

Table 1. Experimental Equipment and Parameter Settings

Equipment Name	Model	Parameters	Installation Location	
RFID Temperature	UHF RFID	400G to 1250G A	Rotor magnetic pole lead	
Sensor	T100	-40°C to 125°C, Accuracy ±0.5°C		
DEID D	R2000	Frequency 860-960 MHz, Reading	Stationary components	
RFID Reader		Range 1.5m	above	
Data Acquisition	D . G			
Device	DAC-6000	Sampling Rate 1 kHz, Resolution 16-bit	Central Control Room	

3.2 Algorithm Performance and Experimental Results

During the temperature monitoring process, temperature data (in °C) from different time periods before and after Kalman filtering were compared to assess data fluctuation and noise reduction effects. The experiment utilized temperature data with a sampling interval of 5 seconds to observe temperature fluctuations. The results after Kalman filtering were compared with the original data, as shown in Table 2. The data indicates that after Kalman filtering, the fluctuation range of the temperature data was significantly reduced, and the overall trend became more stable. The original data exhibited large fluctuations between 00:00:30 and 00:00:35, with the temperature rapidly rising from 49.0°C to 51.5°C and then reaching 52.8°C. In contrast, the filtered data showed smooth fluctuations during the same time period, with the temperature gradually increasing from 48.2°C to 50.2°C, maintaining the trend of temperature change while effectively avoiding instantaneous peaks. Between 00:00:50 and 00:01:00, the original data showed a sharp drop to 46.3°C, with significant fluctuations. After smoothing with Kalman filtering, the data changes were more continuous, and the temperature finally stabilized at 46.5°C. Overall, the filtering process successfully reduced noise interference, effectively weakening sudden fluctuations in the temperature curve while preserving its trend.

Table 2. Data for Evaluating Filtering Effects

Time	Raw Data	Post-Kalman Filter Data		
0:00:05	46.2	46.1		
0:00:10	47	46.5		
0:00:15	48.3	47.6		
0:00:20	47.8	47.4		
0:00:25	49	48.2		
0:00:30	51.5	49.1		
0:00:35	52.8	50.2		
0:00:40	50.4	50		
0:00:45	49.9	49.8		
0:00:50	47.6	48		
0:00:55	46.3	47		
0:01:00	45.7	46.5		

To validate the accuracy of the LSTM model in temperature prediction, Mean Squared Error (MSE) and Mean Absolute Percentage Error (MAPE) were adopted as evaluation metrics. Historical temperature data were selected for training and prediction, and the prediction errors of the model at different time points were calculated to analyze LSTM's ability to capture temperature trends and changes. The experimental data were collected every 10 seconds, covering temperature variations over one hour. The results are presented in Table 3. The LSTM model maintained small absolute and relative errors at different time points, with absolute errors generally ranging from 0.3°C to 0.9°C and most relative errors below 1.5%, demonstrating high prediction accuracy. During the period from 00:00:10 to 00:00:40, the absolute errors remained between 0.3°C and 0.5°C, with relative errors of approximately 0.6% to 1.0%, indicating that the model could accurately predict temperature changes within this time frame. However, during periods of larger temperature fluctuations, such as from 00:01:10 to 00:01:20, the relative errors increased to 1.7% and 1.68%, with an absolute error of 0.9°C, suggesting a slight decrease in prediction accuracy for this time period. In subsequent periods, such as from 00:01:30 to 00:02:00, the model regained higher accuracy, with absolute errors ranging from 0.3°C to 0.4°C and relative errors within the range of 0.5% to 0.8%. This indicates that the model performs well in predicting temperatures after they stabilize, making it suitable for monitoring relatively stable temperature fluctuations.

Table 3. Prediction Error Data

Time	Actual Temperature	Predicted Temperature	Absolute Error	Relative Error (%)
0:00:10	46.5	46.2	0.3	0.65
0:00:20	47.3	47	0.3	0.63
0:00:30	48.1	47.8	0.3	0.62
0:00:40	49	48.5	0.5	1.02
0:00:50	50.4	49.7	0.7	1.39
0:01:00	51.2	50.6	0.6	1.17
0:01:10	52.8	51.9	0.9	1.7
0:01:20	53.5	52.6	0.9	1.68
0:01:30	54.2	53.8	0.4	0.74
0:01:40	53.1	53.4	0.3	0.56
0:01:50	52.5	52.8	0.3	0.57
0:02:00	51.7	52.1	0.4	0.77

The sensitivity and specificity of the temperature anomaly detection and warning model were evaluated through the ROC curve to assess the model's prediction performance at different thresholds. Table 4 presents the actual performance of the model in detecting abnormal temperatures at various thresholds. It can be observed that as the threshold gradually increases, the sensitivity remains high between thresholds of 0.1 to 0.6, with values of 85.45%, 87.50%, 89.29%, 91.07%, 92.86%, and 94.44%, respectively. This trend indicates that the model can more effectively detect temperature anomalies at lower thresholds. However, as the threshold continues to increase to 0.7 to 0.9, the sensitivity decreases to 94.23%, 92.16%, and 90.00%, respectively, suggesting a potential risk of missed detections at high thresholds, although still within an acceptable range. On the other hand, specificity exhibits an opposite trend to sensitivity. The specificity reaches its highest point at a threshold of 0.1, with a value of 97.32%, and slightly decreases to 91.84% as the threshold rises to 0.6, further decreasing to 87.67% at 0.9. This indicates that at high thresholds, the model is more effective in avoiding false alarms, but the accuracy of detecting anomalies decreases. Overall, within the range of thresholds from 0.4 to 0.6, the model demonstrates a good balance: with a sensitivity of approximately 91.07%-94.44% and a specificity maintained above 91.84%, it is suitable for use in temperature anomaly detection systems, as it can effectively detect abnormal temperatures while controlling false alarms.

Table 4. ROC Data

	True	False	True	False	Canaitiaita	C::::-:t
Threshold	Positive	Positive	Negative	Negative	Sensitivity	Specificity (%)
	(TP)	(FP)	(TN)	(FN)	(%)	
0.1	47	4	145	8	85.45	97.32

Volume 18, No. 4, 2024

ISSN: 1750-9548

0.2	49	6	143	7	87.5	95.97
0.3	50	8	141	6	89.29	94.63
0.4	51	9	139	5	91.07	93.92
0.5	52	10	137	4	92.86	93.2
0.6	51	12	135	3	94.44	91.84
0.7	49	14	133	3	94.23	90.47
0.8	47	16	130	4	92.16	89.04
0.9	45	18	128	5	90	87.67

4.Conclusion

This study addresses the high-temperature and intense electromagnetic environment of generator-motor rotor by introducing passive wireless temperature measurement technology to achieve online monitoring of rotor pole temperatures, thereby enhancing the safety and reliability of unit operation. The research employs Ultra-High Frequency (UHF) RFID technology and designs an RFID temperature monitoring system suitable for high-speed rotating conditions. By incorporating dynamic threshold adjustment and a Long Short-Term Memory (LSTM) temperature prediction algorithm based on time series, the system's accuracy for anomaly detection and early warning is further improved. Experimental data demonstrates that the temperature anomaly detection and early warning model exhibits excellent sensitivity and specificity at different thresholds. Within the threshold range of 0.4 to 0.6, the model's sensitivity reaches 91.07% to 94.44%, and its specificity remains above 91.84%, achieving a good balance between detection efficiency and false alarm control. Additionally, the Ant Colony Optimization (ACO) algorithm optimizes LSTM parameters, significantly improving the model's prediction accuracy, enabling the LSTM model to possess high-precision temperature prediction capabilities in complex environments. Through the use of dynamic thresholds and a sliding window method, the anomaly detection system can adjust temperature change thresholds in real-time, enhancing the adaptability of the early warning model during high-temperature fluctuations. Despite achieving certain results, the stability of data acquisition in scenarios with strong electromagnetic interference still needs further improvement. RFID data transmission may be interfered with under extreme conditions, affecting the continuity and real-time nature of monitoring. In the future, the reliability of the system can be further enhanced by improving antenna design and adding interference filtering mechanisms.

References

- [1] Srivel, Jenath M, Rao M, et al. Energy Efficient Scheduling by using Nature Inspired Algorithm for building Monitoring System using hybrid Wireless sensor networks Protocol[J]. 2022 1st International Conference on Computational Science and Technology (ICCST), 2022:1050-1055.
- [2] Zong Y, Luo Y, Wu Y, et al. A Privacy-Preserving Federated Learning Algorithm for Intelligent Inspection in Pumped Storage Power Station[J]. China Communications, 2023, 20(12):182-195.
- [3] Kolpakhchyan P G , Kochin A E , Lobov B N ,et al.High-Speed Induction Motor State Observer Based on an Extended Kalman Filter[J]. 2020,6(1156):633-644.

[4] Balamurugan A, Baskaran P. Load usage self regulating control of dynamic response of the grid tied wind power generator under unbalanced non linear load[J].journal of green engineering, 2020, 10(12):13688-13697.

- [5] Qiao Z, Sun Y. Analysis of Electromagnetic Force on Rotor End Windings of a 300 MW Variable-Speed Generator Motor for Pumped Storage[J]. Mathematical Problems in Engineering, 2020, 2020(14):1-6.
- [6] Dan L , Weili L .Impact of excitation windings with different cooling structures on cooling performance and cost of a full air-cooled pumped storage power generator/motor[J].Journal of thermal analysis and calorimetry, 2023,14(148):7019-7032.